Experimental Validation of Harmonic Impedance Measurement and LTP Nyquist Criterion for Stability Analysis in Power Converter Networks

Valerio Salis, *Member, IEEE,* Alessandro Costabeber, *Member, IEEE,* Stephen M. Cox

Francesco Tardelli and Pericle Zanchetta, *Senior Member, IEEE*

Abstract

This paper presents the first experimental validation of the stability analysis based on the online measurement of harmonic impedances exploiting the Linear Time Periodic (LTP) approach, applied to AC networks of power converters. Previous publications have provided the theoretical framework for the method, enabling the stability assessment of an unknown system adopting a black-box approach, relying only on injected perturbations and local measurements. The experimental case study considered in this paper comprises two single-phase converters, one acting as *source subsystem* and the other as *load subsystem*. A third converter, the *Stability Measurement Unit* (SMU), is controlled to inject small current perturbations at the point of common coupling (PCC). From the measured small-signal perturbations of PCC voltage, source current and load current, the harmonic impedances of source and load subsystems are calculated. The LTP Nyquist Criterion is then applied to the ratio of the two harmonic impedances in order to assess the stability of the whole system. Theoretical and experimental results from a 5 kW laboratory prototype are provided and confirm the effectiveness of the method. In addition, the measurements do not require sophisticated equipment or control boards and can be easily performed from data sampled by commercial micro-controllers.

Index Terms

Linear Time Periodic Systems, Harmonic State Space Model, Harmonic Impedances, LTP Nyquist Criterion, Stability Analysis

I. Introduction

STABILITY analysis of interconnected power systems has been an interesting and challenging topic for researchers in the past decades, and it is still nowadays an open field for research [1], [2]. One of the first investigations presented in the literature was provided by Middlebrook [3], who analysed the instability issues due to interactions between DC/DC converters and their input filters. The linearised input and output impedances of the system were first evaluated and the Nyquist Criterion was then applied to assess the stability of the system. This approach was then extended to AC power converters by

V. Salis, A. Costabeber, F. Tardelli and P. Zanchetta are with the Department of Electrical and Electronic Engineering, University of Nottingham, Nottingham NG7 2RD, U.K. (e-mail: valerio.salis@nottingham.ac.uk).

S. M. Cox is with the School of Mathematical Sciences, University of Nottingham, Nottingham NG7 2RD, U.K.

Belkhayat [4], with focus on balanced three-phase AC systems. Exploiting the Park transformation, the system is represented in dq reference frame, hence becoming a MIMO linear system. Then, stability is assessed by applying the Generalised Nyquist Criterion [5].

This, however, is only one of the possible stability-assessment methods [6]. With a focus on balanced three-phase systems, other approaches are: *Harmonic Linearisation* [7], where a small-signal perturbation is injected into the system in order to measure the small-signal source and load impedances. Stability is then assessed based on the ratio of the two impedances. *Dynamic Phasors*, with extension to multi-source and multi-frequency scenarios [8]. *DQ-reference frame* [9], where it has been demonstrated that for a high power factor system, the only relevant impedance matrices are the dd and qq ones, allowing a simplification of the whole system as two decoupled DC subsystems. *Sequence Domain Method* [10], which is based on the calculation of the positive and negative sequence impedances and has a relevant connection with the dq-frame approach [11]. *Unified Impedance Model* [12], where the system impedances and calculations are proposed in the $\alpha\beta$-domain. Finally, the *Harmonic State Space*, where one of the advantages is that also the switching behaviour can be taken into account in the analysis [13].

In general, some of the aforementioned approaches cannot be directly applied to analyse single-phase systems. In this case, the Dynamic Phasor method can be used considering the real and imaginary parts of the phasor in order to build 2×2 impedance matrices and use the Generalised Nyquist Criterion [14]. Also the Harmonic Linearisation method [15] can be applied following a similar approach. In the Apparent Impedance method [16], only the impedance at the measuring point is evaluated, it being effectively a closed-loop transfer function that contains information about stability. Another option is the Harmonic Linearisation defined using signal-flow graphs [17], providing a visual tool in order to understand the various harmonic interactions. Harmonic State Space, which is based on the Linear Time Periodic (LTP) systems theory [18], [19], [20], also provides a straightforward relationship between the various harmonic components of the system.

Focusing on a single-phase scenario, this paper proposes the experimental validation of the Harmonic State Space (HSS) method in combination with the LTP Nyquist Criterion, already presented in detail in [21]. In the previous publication, the ability of the method to assess stability of a black-box single-phase AC system was demonstrated theoretically and in simulation but not experimentally. To fill the gap and prove the practical feasibility of the method, this paper presents its experimental implementation in the same system configuration as discussed in [21]. The case study includes a source and load converter: the source controls the AC voltage of the network and the load controls the current absorbed with unity power factor. The Harmonic Impedances of both subsystems are measured through small-signal current perturbations injected at the PCC by a third converter referred to as the SMU – Stability Measurement Unit. Then the LTP Nyquist Criterion is applied to the ratio of the two Harmonic Impedances in order to assess the stability of the whole system.

The comparison with other existing techniques, the theoretical analysis and an extensive set of simulation results have been already presented in [21]. Hence, this paper is solely intended to discuss the experimental validation of the method. For this reason, the focus will be more on the practical aspects required to apply the technique and replicate the results rather than on the theoretical details, for which the reader is invited to refer to [21].

This paper is organised as follows: Section II describes the AC system under analysis and the SMU; Section III provides

a practical review of LTP theory and the Harmonic Impedance measurement method; Section IV presents an extensive set of experimental results from the case study; Section V discusses advantages and challenges and Section VI concludes the paper.

II. Experimental system: source, load and SMU converters

The case study for the experimental validation of the stability analysis based on LTP Nyquist Criterion and Harmonic Impedances is reported in Fig. 1, and is the same as used in [21]: a source converter with inner current loop and outer voltage loop that controls the PCC voltage and a load converter that draws a controlled current synchronised with the PCC voltage via a DQ Phase-Locked Loop (PLL). Compared to the system in [21], the small current injection is now implemented by a real converter with closed-loop current control (SMU).

From Fig. 1 it can be seen that control complexity has been deliberately kept to the bare minimum, using only PI controllers and feed-forward terms. The reason is that the focus of the work is on the implementation of the black-box stability analysis method rather than on the performances of the AC system, which is generally unknown to the SMU. In addition, showing that the method is effective even with a simple hardware and control architecture for the SMU demonstrates its ease of implementation, which does not require complex hardware or sophisticated controllers for current injection.

The load and source H-bridge converters are custom designs using IXYS $IXFK120N65X2$ power mosfets switching at $f_{pwm}^{source/load} = 10$ kHz. The load current has been limited to $i_{rms}^{load} = 30$ A. Three-level modulation is used with double update at 20 kHz, also corresponding to the sampling frequency. All the controllers for source and load converter are implemented in the same control platform, a Texas C6713 DSP with custom FPGA interface, and have been designed in the continuous time domain (as in [21] and in Fig. 1) for a phase margin $PM = 60^o$ and later discretised using the Tustin method. Source

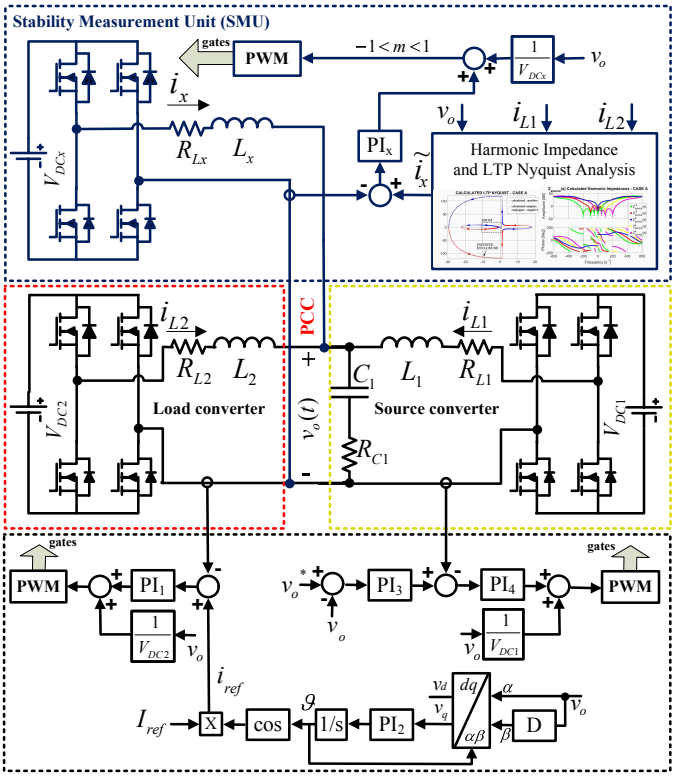

Fig. 1. Case study: single-phase power-converter-based AC network with Stability Measurement Unit (SMU).

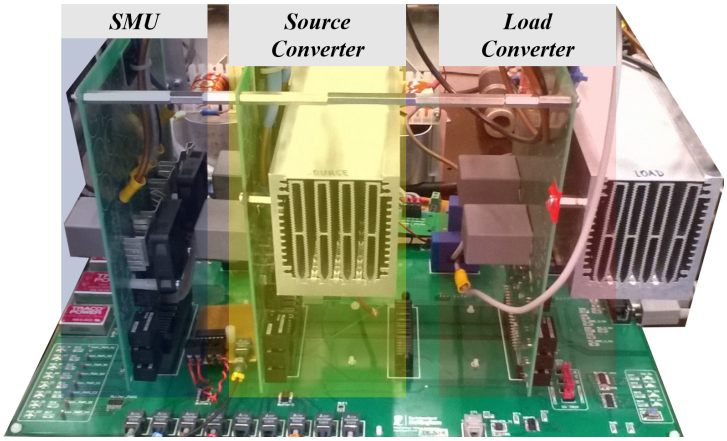

Fig. 2. Experimental rig.

converter bandwidths are $BW_i^{source} = 830$ Hz and $BW_v^{source} = 333$ Hz for current and voltage loop respectively. Load converter current bandwidth is $BW_i^{load} = 1$ kHz and PLL bandwidth is $BW_{PLL} = 5$ Hz.

To minimise complexity, the SMU H-bridge uses the same power boards developed for the source and load converters but replacing the switches with Infineon $IPX65R110CFD$ mosfets switching at $f_{pwm}^{SMU} = 20$ kHz. Also here three-level modulation is used with double update and sampling at 40 kHz. The SMU is controlled by a Texas $F28377S$MCU completely independent from the source-load controller. The current control has been designed for $PM = 60^o$ and $BW_i^{SMU} = 2$ kHz. The SMU is also connected to a host PC, which through a dedicated Matlab script provides the reference signal for the injections, stores the measured signals with a 20 kHz sampling frequency (one every two samples used by the SMU current control) and finally calculates the LTP Nyquist plot once all the data is collected. The scope of this first implementation is to validate the proposed impedance measurement method and demonstrate that measurements are feasible in practice also having a relatively simple hardware and control software. On the other hand, the SMU has been designed as a fully independent and automated unit, to be as close as possible to a dedicated measurement equipment. The SMU itself, its control and the overall implementation of the harmonic impedance measurement can be greatly improved in terms of measurement speed, data storage requirements, signal to noise ratio and minimum amplitude of injected signal to obtain correct results. All these analyses and optimisations are currently ongoing.

A photo of the experimental rig, excluding the controllers, is shown in Fig. 2. The remaining system parameters, including the controller gains referred to the continuous-time control design, are reported in Table I. Some of the parameters are slightly different from those previously used in [21] due to laboratory constraints.

In order to avoid repetition, the system equations and most of the LTP theoretical analysis will not be reported in this paper and the reader is invited to refer to [21] for a detailed analysis.

III. Basic Practical Review of LTP Theory

In this Section the basic tools required to perform LTP stability analysis are briefly discussed. For a detailed review, the reader should refer to the original formulation presented by Wereley and Hall [22], [23]. Given the single-phase system in Fig.

TABLE I. Experimental System Parameters

Voltages	$v_o^*(t) = 115\sqrt{2}\sin(2\pi 50t)$ V, $f_g = 50$ Hz $V_{DC1} = V_{DC2} = V_{DC3} = 250$ V
Current	$i_{ref}(t) = -I_{ref}\cos(\theta)$ A, θ from PLL minus sign: power-flow towards load
PWM and sampling	$f_{pwm}^{source/load} = 10$ kHz, $f_s^{source/load} = 20$ kHz $f_{pwm}^{SMU} = 20$ kHz, $f_s^{SMU} = 40$ kHz Dead-Time T_{dt}=1 μs (not compensated)
Filters	$L_1 = 2.9$ mH, $R_{L1} = 0.26\ \Omega$, $C_1 = 22\ \mu$F, $R_{C1} = 0.7\ \Omega$, $L_2 = 0.88$ mH, $R_{L2} = 0.1\ \Omega$, $L_x = 20$ mH, $R_{Lx} = 0.29\ \Omega$
Controllers in Fig. 1	$[k_{p1}, k_{i1}]$ = [0.022,10.95], $[k_{p2}, k_{i2}]$ = [27.2,493.48] $[k_{p3}, k_{i3}]$ = [0.043,55.77], $[k_{p4}, k_{i4}]$ = [0.061,49.20] $[k_{px}, k_{ix}]$ = [1,700], $D \rightarrow$ see [21]

1, the linearisation around its steady-state leads to the Linear Time Periodic (LTP) model

$$\dot{\tilde{x}}(t) = A(t)\tilde{x}(t) + B(t)\tilde{u}(t), \quad \tilde{y}(t) = C(t)\tilde{x}(t) + D(t)\tilde{u}(t), \tag{1}$$

where $A(t)$, $B(t)$, $C(t)$ and $D(t)$ are T-periodic, and T is the period of the steady-state, $T = 1/f_g = 20ms$ in the case study. Exploiting the Exponentially Modulated Periodic (EMP) signal and the Toeplitz transformation, the Harmonic State-Space Model (HSSM) of the system is derived as

$$s\mathcal{X} = (\mathcal{A} - \mathcal{N})\mathcal{X} + \mathcal{B}\mathcal{U}, \quad \mathcal{Y} = \mathcal{C}\mathcal{X} + \mathcal{D}\mathcal{U}, \tag{2}$$

with $\mathcal{N} = \text{diag}(\dots, N_{-n}, \dots, N_{-1}, N_0, N_1, \dots, N_n, \dots)$, N_n being a diagonal square matrix of the same dimension as A_n with diagonal coefficients equal to $jn\omega_g$. $\mathcal{A}$ is the Toeplitz transform of A, defined as

$$\mathcal{A} = \mathcal{T}\Big[\overbrace{\sum_{n=-M}^{+M} A_n e^{jn\omega_g t}}^{A(t)}\Big] = \begin{bmatrix} & \vdots & \vdots & \vdots & \\ \cdot\cdot & A_0 & A_{-1} & A_{-2} & \cdot\cdot \\ \cdot\cdot & A_1 & A_0 & A_{-1} & \cdot\cdot \\ \cdot\cdot & A_2 & A_1 & A_0 & \cdot\cdot \\ & \vdots & \vdots & \vdots & \end{bmatrix}, \tag{3}$$

where M is the truncation order limiting the dimension of $\mathcal{A}$ to $2M+1$. The same considerations hold for $\mathcal{B}$, $\mathcal{C}$, $\mathcal{D}$. Stability analysis could now be performed by evaluating the eigenvalues of the $\mathcal{A} - \mathcal{N}$ matrix. However this requires a knowledge of the system parameters, which is not available when a black-box assessment is required.

From (2), the Harmonic Transfer Function (HTF) of the LTP system is defined through

$$\mathcal{Y} = \mathcal{H}(s)\mathcal{U}, \quad \mathcal{H}(s) = \mathcal{C}\left[s\mathcal{I} - (\mathcal{A} - \mathcal{N})\right]^{-1}\mathcal{B} + \mathcal{D}. \tag{4}$$

In order to apply the LTP Nyquist Criterion and assess stability with a black-box approach, the Harmonic Impedances must be measured. To do so, a small-signal current perturbation is injected by the SMU at the PCC, as in Fig. 3. The impact of

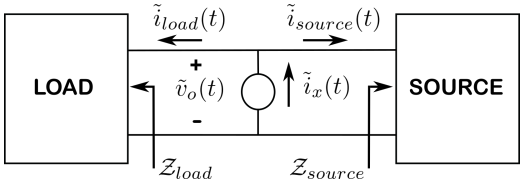

Fig. 3. Small-signal current injection at the PCC and harmonic impedances.

an injected perturbation into the system requires careful consideration. In fact, when $\tilde{i}_x(t) = I_x \cos(\omega_{inj} t)$ is injected by the SMU, the PCC voltage and the source/load current perturbations can be written in Fourier form with truncation order M:

$$\tilde{p}(t) = \sum_{n=-M}^{+M} \tilde{p}_n e^{j(\omega_{inj} + n\omega_g)t}, \tag{5}$$

with $\tilde{p}(t) = \tilde{v}_o(t),\ \tilde{i}_{source}(t),\ \tilde{i}_{load}(t)$, respectively. Thus, the source harmonic impedance at ω_{inj} satisfies

$$\begin{bmatrix} \tilde{v}_{o,-M}(\omega_{inj}) \\ \vdots \\ \tilde{v}_{o,-1}(\omega_{inj}) \\ \tilde{v}_{o,0}(\omega_{inj}) \\ \tilde{v}_{o,+1}(\omega_{inj}) \\ \vdots \\ \tilde{v}_{o,+M}(\omega_{inj}) \end{bmatrix} = \mathcal{Z}_{source}(j\omega_{inj}) \begin{bmatrix} \tilde{i}_{source,-M}(\omega_{inj}) \\ \vdots \\ \tilde{i}_{source,-1}(\omega_{inj}) \\ \tilde{i}_{source,0}(\omega_{inj}) \\ \tilde{i}_{source,+1}(\omega_{inj}) \\ \vdots \\ \tilde{i}_{source,+M}(\omega_{inj}) \end{bmatrix}, \tag{6}$$

with $\omega_{inj} \in (-\omega_g/2, +\omega_g/2)$ [21]. Written in a more compact notation, $v_o(\omega_{inj}) = \mathcal{Z}_{source}(j\omega_{inj}) i_{source}(\omega_{inj})$, and also $v_o(\omega_{inj}) = \mathcal{Z}_{load}(j\omega_{inj}) i_{load}(\omega_{inj})$.

In general, the harmonic impedance will be of the form (7), which is a square matrix of dimension $2M+1$ and where x stands for either $source$ or $load$. A possible solution to measure these impedances at the frequency ω_{inj}, is to perform a set of $2M+1$ independent small-signal current injections:

- *n=1*: the first injection is $\tilde{i}_x(t) = I_x \cos((\omega_{inj} - M\omega_g)t)$. $\tilde{v}_o(t),\ \tilde{i}_{source}(t),\ \tilde{i}_{load}(t)$ are measured and represented by their Fourier series as in (5) and their complex harmonic coefficients are collected into the column vectors $v_o^{(-M)}(\omega_{inj})$, $i_{source}^{(-M)}(\omega_{inj})$, $i_{load}^{(-M)}(\omega_{inj})$ as in (6).
- $\cdots$
- *n=M+1*: the intermediate injection is $\tilde{i}_x(t) = I_x \cos(\omega_{inj} t)$, and the perturbed signals provide the vectors $v_o^{(0)}(\omega_{inj})$, $i_{source}^{(0)}(\omega_{inj})$, $i_{load}^{(0)}(\omega_{inj})$ as in (6).
- $\cdots$
- *n=2M+1*: the last injection is $\tilde{i}_x(t) = I_x \cos((\omega_{inj} + M\omega_g)t)$, and the perturbed signals provide the vectors $v_o^{(+M)}(\omega_{inj})$, $i_{source}^{(+M)}(\omega_{inj})$, $i_{load}^{(+M)}(\omega_{inj})$ as in (6).

$$\mathcal{Z}_x(j\omega_{inj}) = \begin{bmatrix} \mathcal{Z}_x^0(j(\omega_{inj}-M\omega_g)) & \cdots & & & & & \\ \vdots & \ddots & \ddots & \ddots & & & \\ & \mathcal{Z}_x^0(j(\omega_{inj}-1\omega_g)) & \mathcal{Z}_x^{-1}(j\omega_{inj}) & \mathcal{Z}_x^{-2}(j(\omega_{inj}+1\omega_g)) & & & \\ & \mathcal{Z}_x^1(j(\omega_{inj}-1\omega_g)) & \mathcal{Z}_x^0(j\omega_{inj}) & \mathcal{Z}_x^{-1}(j(\omega_{inj}+1\omega_g)) & & & \\ & \mathcal{Z}_x^2(j(\omega_{inj}-(1)\omega_g)) & \mathcal{Z}_x^1(j\omega_{inj}) & \mathcal{Z}_x^0(j(\omega_{inj}+(1)\omega_g)) & & & \\ & \ddots & \ddots & \ddots & \vdots & & \\ & & & & \cdots \mathcal{Z}_x^0(j(\omega_{inj}+M\omega_g)) & & \end{bmatrix} \tag{7}$$

These vectors are then rearranged into matrices as

$$\begin{aligned} \mathcal{V}_o(\omega_{inj}) &= \begin{bmatrix} v_o^{(-M)} & \cdots & v_o^{(0)} & \cdots & v_o^{(+M)} \end{bmatrix} \\ \mathcal{I}_{source}(\omega_{inj}) &= \begin{bmatrix} i_{source}^{(-M)} & \cdots & i_{source}^{(0)} & \cdots & i_{source}^{(+M)} \end{bmatrix} \\ \mathcal{I}_{load}(\omega_{inj}) &= \begin{bmatrix} i_{load}^{(-M)} & \cdots & i_{load}^{(0)} & \cdots & i_{load}^{(+M)} \end{bmatrix} \end{aligned} \tag{8}$$

and finally the source and load harmonic impedances at ω_{inj} are calculated as

$$\begin{aligned} \mathcal{Z}_{source}(j\omega_{inj}) &= \mathcal{V}_o(\omega_{inj})\left[\mathcal{I}_{source}(\omega_{inj})\right]^{-1} \\ \mathcal{Z}_{load}(j\omega_{inj}) &= \mathcal{V}_o(\omega_{inj})\left[\mathcal{I}_{load}(\omega_{inj})\right]^{-1}. \end{aligned} \tag{9}$$

This procedure has to be performed for each $\omega_{inj} \in (-\omega_g/2, \omega_g/2)$ that has been chosen to reconstruct the LTP Nyquist plot experimentally.

Now, from Fig. 3, the LTP Nyquist plot is obtained by evaluating the eigenvalues of the open-loop HTF $\mathcal{F}(j\omega_{inj})$, which is equal either to $\mathcal{F}(j\omega_{inj}) = \left[\mathcal{Z}_{source}(j\omega_{inj})\right]^{-1}\mathcal{Z}_{load}(j\omega_{inj})$ or $\mathcal{F}(j\omega_{inj}) = \left[\mathcal{Z}_{load}(j\omega_{inj})\right]^{-1}\mathcal{Z}_{source}(j\omega_{inj})$. The stability of the system is assessed using the following theorem.

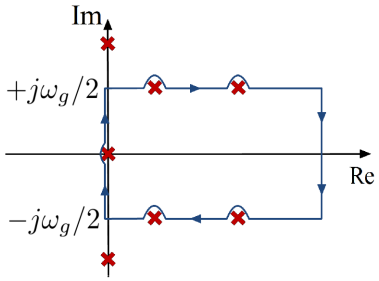

Fig. 4. LTP Nyquist contour plot in the complex plane. Red crosses - poles of the open-loop HTF, either $\mathcal{Z}_{source}^{-1}(s)\mathcal{Z}_{load}(s)$ or $\mathcal{Z}_{load}^{-1}(s)\mathcal{Z}_{source}(s)$.

Theorem: consider the open-loop harmonic transfer function $\mathcal{F}(j\omega_{inj})$ and assume that it has no unobservable or uncontrollable right-half-plane poles. Then, the LTP system (1) is stable if and only if the LTP Nyquist plot of the eigenvalues of $\mathcal{Z}_{source}^{-1}(s)\mathcal{Z}_{load}(s)$ (or $\mathcal{Z}_{load}^{-1}(s)\mathcal{Z}_{source}(s)$), for $s = j\omega$ and $\omega \in [-\omega_g/2, \omega_g/2]$, has a number of counter-clockwise encirclements of the critical point $(-1, 0)$ in the complex plane equal to the number of poles of $\mathcal{Z}_{source}^{-1}(s)\mathcal{Z}_{load}(s)$ (or $\mathcal{Z}_{load}^{-1}(s)\mathcal{Z}_{source}(s)$), included within the LTP Nyquist contour plot, as shown in Fig. 4 [22].

IV. Experimental Black-Box Stability Assessment

In this section, the Harmonic Impedance measurement method and the LTP Nyquist Criterion discussed in Section III are applied to the experimental case study discussed in Section II. The proposed method has been developed as a black-box stability assessment, since it relies only on current injections and measured perturbations and does not require any of the system parameters. For the sake of completeness, the results of the black-box stability assessment are also compared with the analytical prediction based on the nominal values of the system parameters and on the LTP model in [21]. In the following, two configurations are analysed:

- *CASE A*: stable mode with the parameters in Table I;
- *CASE B*: bounded unstable mode, with a steady-state high-frequency oscillation in all the waveforms.

The experimental measurement of the Harmonic Impedances has been performed as discussed in Section III. ω_{inj} has been selected from $[2, 3, 4, 5, 6, 8, 10, 12, 15, 20]$ Hz, which identifies 10 groups of independent measurements. Each single group comprises $2M + 1$ separate injections, with M chosen equal to 27. The first group, with $\omega_{inj} = 2$ Hz, thus comprises 55 different injections, i.e. $\mathrm{abs}(-1350 + 2)$ Hz, $\mathrm{abs}(-1300 + 2)$ Hz, ..., $\mathrm{abs}(1300 + 2)$ Hz, $\mathrm{abs}(1350 + 2)$ Hz, and it allows measurement of the Harmonic Impedances at $\mathrm{abs}[2 + m(\pm 50)]$ Hz, with $m = 0, 1, 2, \ldots, 27$. Similar considerations hold for the other injected frequencies.

To evaluate the quality of the experimental stability assessment, analytical calculations have been performed using the LTP model of the system (1)–(4), using the nominal parameters and truncating at $M = 80$. The Harmonic Impedances have been calculated by injecting frequencies equal to $\omega_{inj} = 2\pi[-24.9, -24.8, \ldots, -0.1, 0.1, \ldots, 24.8, 24.9]$ rad/s.

It is important to highlight that the set of frequencies in which the harmonic impedance in (6) is measured, i.e. $[2 - 20]$ Hz for the experiment and $[-24.9, 24.9]$ Hz for the simulations, should not be confused with the frequency range in which the individual impedances are estimated. In fact, the two ranges are related through the truncation order M: each point measured in the first range generates a greater number of points in the second range. In the range considered for the experimental validation, each ω_{inj} leads to $\mathrm{abs}[\omega_{inj} + m(\pm 2\pi 50)]$ rad/s, with $m = 0, 1, 2, \ldots, 27$ in the individual impedances. It is also worth remembering that the LTP Nyquist plot for the range $[-\omega_g/2, 0]$ is the complex conjugate of the one for $[0, +\omega_g/2]$, so only the evaluation of the latter is required.

In the following subsections, the two cases will be evaluated starting from the analytical prediction and comparing it with the stability measured with the black-box approach, estimating the Harmonic Impedances and applying the LTP Nyquist Criterion.

CASE A - Stable System

In this configuration the system works in a stable operating mode, with the parameters reported in Table I. The currents i_{L1}, i_{L2} and voltage v_o are reported in Fig. 5.

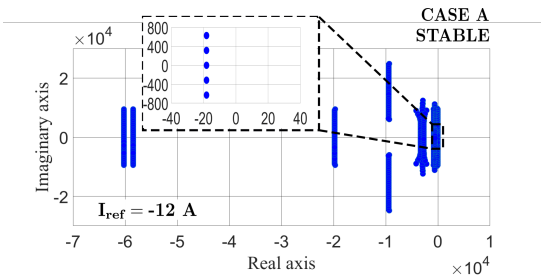

Fig. 6. LTP eigenvalue loci plot from the analytical model - CASE A.

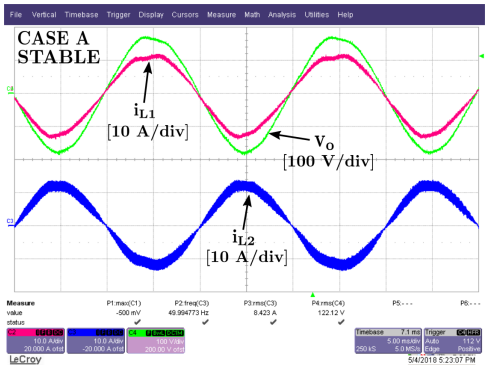

Fig. 5. Experimental data [5 ms/div] - CASE A. Currents: pink - i_{L1}, blue - i_{L2}; voltage: green - v_o - steady-state waveforms with SMU off.

The stability of this operating mode is confirmed by the analytical LTP eigenvalue loci in Fig. 6, calculated by feeding the nominal system parameters in the model derived in [21]. As shown in the figure, all the eigenvalues lie on the left-hand side of the complex plane. It is worth noting that this analytical prediction is not required by the black-box stability assessment method and has been presented here only to compare the experimental results with a theoretical prediction.

In order to apply the LTP Nyquist Criterion, first the Harmonic Impedances, $\mathcal{Z}_{source}(s)$ and $\mathcal{Z}_{load}(s)$, are experimentally measured using the small-signal current injection method previously described. As examples of waveforms during the injection, Fig. 7-(a) shows the current and voltage waveforms when the SMU is injecting 1 A peak at 6 Hz, and Fig. 7-(b) when the SMU injects 1 A peak at 606 Hz. The point-to-point measured Harmonic Impedances are reported in Fig. 8, where we show only those up to order ± 4 for the sake of clarity.

The set of required injections is programmed into the SMU controller and the measured perturbations are logged and post-processed in Matlab to calculate the impedances. Then, the Harmonic Impedances are used to evaluate the open-loop harmonic transfer function $\mathcal{F}(s) = \mathcal{Z}_{source}(s)^{-1}\mathcal{Z}_{load}(s)$, which is shown in Fig. 9. The location of the poles of $\mathcal{F}(s)$ is important to determine the number of counterclockwise encirclements that the LTP Nyquist plot must perform around the critical point $(-1, 0)$ for a stable system. Since the HTFs are measured point-to-point, a closed-form expression to calculate the poles is not available. The solution adopted in this paper to overcome this limitation is to perform a curve-fitting of the single HTFs shown in Fig. 9. In the case study, only the 0-component of $\mathcal{F}(s)$, i.e. $\mathcal{F}_0(s)$, shows poles that lie inside the LTP Nyquist Contour plot, and therefore the other components will not be discussed further. However, in general the poles of all the components of $\mathcal{F}(s)$ must be checked. The fitting has been based on the package provided by Gustavsen [24], [25] and is reported in Fig. 10, from which it is possible to locate the poles of interest, shown in Fig. 11. It can be seen that $\mathcal{F}_0(s)$ has a pole at the origin and a pair of complex-conjugate poles at $s = 53.2 \pm j2\pi 50$. $\mathcal{F}_0(s + j\omega_g)$ has the same poles as $\mathcal{F}_0(s)$ but with a shift equal to

$+j\omega_g$, meaning that it has poles at $s = 53.2$, $s = 53.2 + 2j2\pi50$ and $s = j2\pi50$. Similar considerations apply to $\mathcal{F}_0(s - j\omega_g)$. Hence, the poles of $\mathcal{F}(s)$ that are inside the LTP Nyquist Contour are $s = 0$ and $s = 53.2$, so the system is stable if the LTP Nyquist plot has two counterclockwise encirclements of the critical point $(-1, 0)$. Please note that the phase of $\mathcal{F}_0(s)$ starts from a value close to -180^o, which is due to a pole located in $s = -1.22$. However, the magnitude of $\mathcal{F}_0(s)$ has an initial slope of -20 dB/dec, confirming the presence of only one pole in the origin.

Finally, the LTP Nyquist plots for Case A are shown in Fig. 12: (a) and (b) show the experimentally measured plot and (c), (d) the one calculated with the analytical model from [21]. As can be seen, the outer encirclement is derived with an infinite enclosure. For each pole at the origin of $\mathcal{F}(s)$ (there is a single such pole in the present case study) half a circle must be added between the diverging lines of the LTP Nyquist curve, according to the LTP Nyquist theory. The inner counterclockwise encirclement, shown in the zooms in (b) and (d), provides the second required encirclement, which confirms the stability of the system. The comparison between the zoomed plots in (b) and (d) also shows that the experimentally measured LTP Nyquist is consistent with the analytical one, even though a full match is not to be expected since the analytical one is based on nominal system parameters that may differ from the actual ones in the experimental rig.

CASE B - Bounded Unstable System

In the second case under analysis, the system is in a bounded unstable operating mode, obtained by reducing the phase margin of the load converter current control. The only difference with the parameters reported in Table I is that the integral gain k_{i1} has been increased to $k_{i1} = 490$. The currents i_{L1}, i_{L2} and voltage v_o when the SMU is off are reported in Fig. 13,

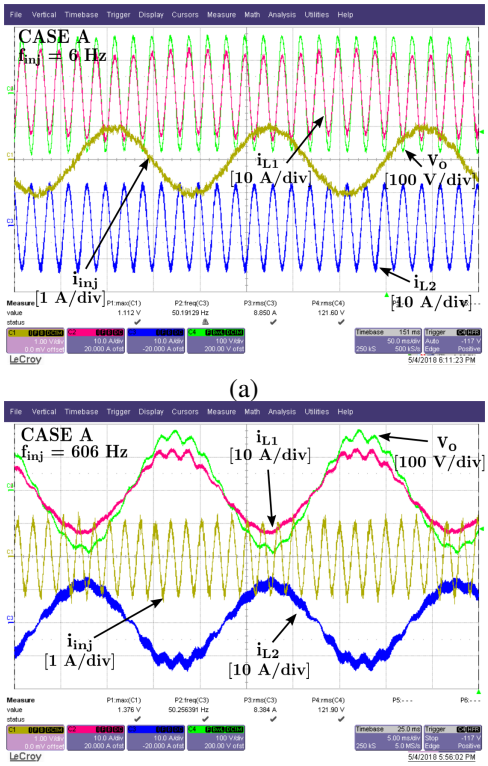

Fig. 7. Experimental data [5 ms/div] - CASE A. Currents: pink - i_{L1}, blue - i_{L2}, yellow - i_{inj}; voltage: green - v_o. Current injection at (a) - 6 Hz; (b) - 606 Hz.

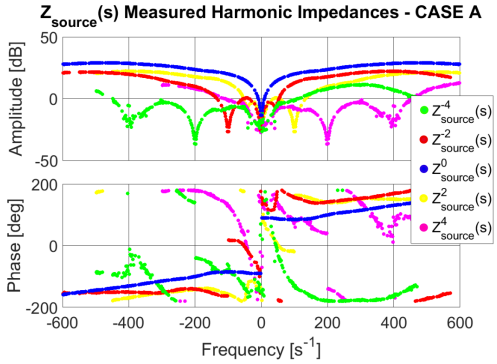

(a)

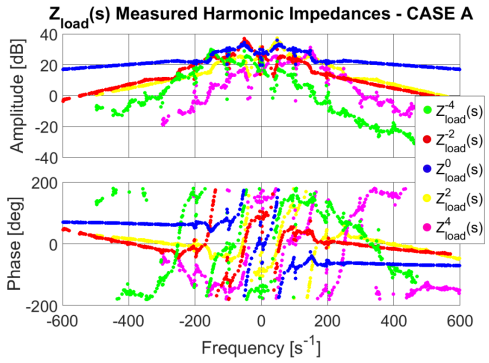

(b)

Fig. 8. Experimental data: (a) Source and (b) Load Measured Harmonic Impedances - CASE A.

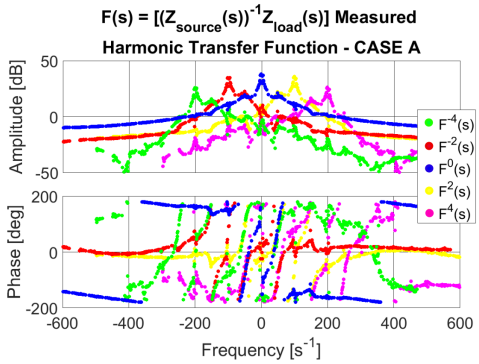

Fig. 9. Experimental data: measured Open-Loop HTF $\mathcal{F}(s)$ - CASE A.

where it can be seen that a steady-state high-frequency oscillation affects all the waveforms of the system. Such instability does not diverge and hence does not cause tripping of the protections. The experimental evaluation of Case B follows the same steps as the one proposed for Case A.

The unstable operating mode is also confirmed by the analytical calculation of the LTP eigenvalue loci, shown in Fig. 14, where some of the eigenvalues lie on the right-hand side of the complex plane.

As in Case A, the first step to determine the LTP Nyquist plot is to measure the source and load Harmonic Impedances. Fig. 15 shows the current and voltage waveforms when the SMU is injecting a 1 A peak current perturbation at (a) 6 Hz and (b) 606 Hz, as examples of the current injections performed with the SMU. It can be seen that the amplitude of the oscillations induced by the injection is bigger compared to the amplitude of those in the stable case (Fig. 7), which is consistent with

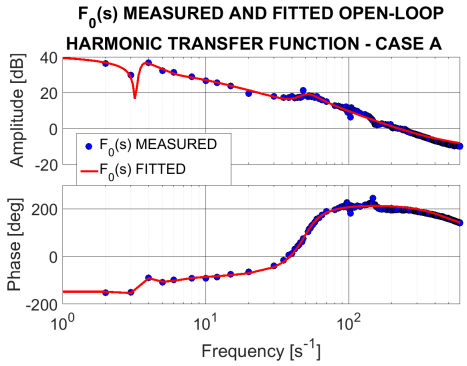

Fig. 10. Experimental data: measured (dots) and fitted (line) Open-Loop HTF $\mathcal{F}_0(s)$ - CASE A.

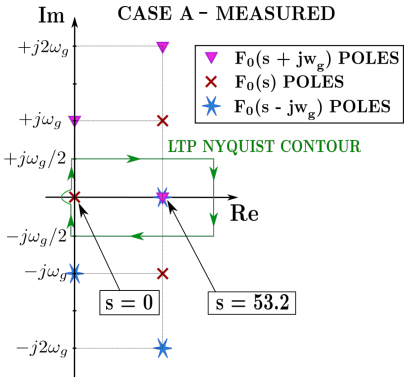

Fig. 11. Experimental data: measured pole location of the Open-Loop HTF $\mathcal{F}_0(s)$ - two poles inside the LTP Nyquist Contour - CASE A.

the unstable nature of the system in this case. The point-to-point measured Harmonic Impedances are reported in Fig. 16. An interesting feature that is worth pointing out is that the difference between the stable and unstable case is solely due to the change in the integral gain of the load current control. However, this change also has the consequence that the source harmonic impedance is different in the two cases, since the harmonic impedances are small-signal models and they change with a change in the steady-state trajectory of the system.

The Open-Loop HTF $\mathcal{F}(s)$ is shown in Fig. 17, and again the fitting of only the 0-component $\mathcal{F}_0(s)$ is provided in order to evaluate the open-loop poles and determine the number of encirclements for the LTP Nyquist plot. This fitting is reported in Fig. 18, and the open-loop poles are shown in Fig. 19, where it can be seen that for the unstable case there is only one pole inside the LTP Nyquist Contour, which is a pole at the origin.

Hence, the system is stable if the LTP Nyquist plot provides one counterclockwise encirclement of the point $(-1, 0)$. However, as shown in the experimentally measured and analytically calculated LTP Nyquist plots reported in Fig. 20, no encirclements of the critical point are made, confirming the unstable nature of the system in Case B.

V. Discussion

The main advantage of the proposed stability analysis based on the measurement of Harmonic Impedances and LTP Nyquist Criterion is that it is general and can be applied to different power electronic systems, both single-phase and three-phase, balanced or unbalanced. In addition, the experimental validation provided in this paper demonstrates that the method is fairly robust against implementation accuracy, since a good match with a theoretical prediction can be obtained with a simple

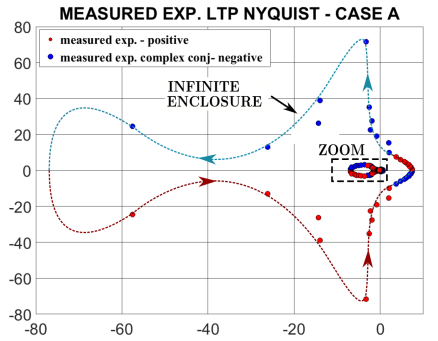

(a)

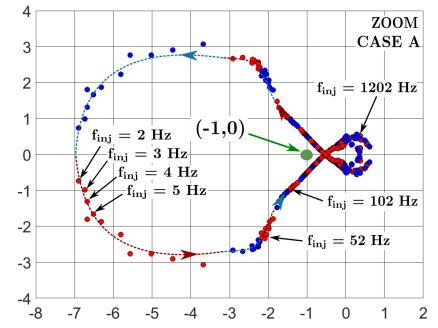

(b)

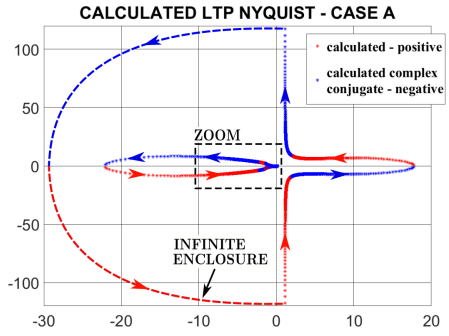

(c)

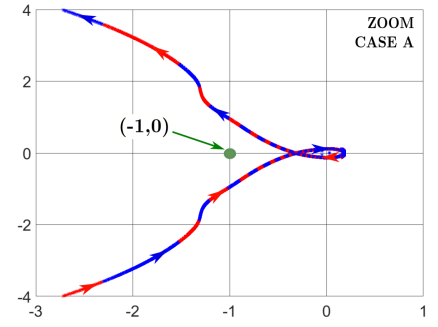

(d)

Fig. 12. (a)-(b) Measured LTP Nyquist plot and (c)-(d) analytical prediction of the LTP Nyquist plot. Two counterclockwise encirclements of the critical point - stable system - CASE A.

implementation of the SMU for current injection, without the need for sophisticated control structures or high bandwidth current measurements.

Compared with other methods, like Harmonic Linearisation or Dynamic Phasor, the main advantage provided by the HSS

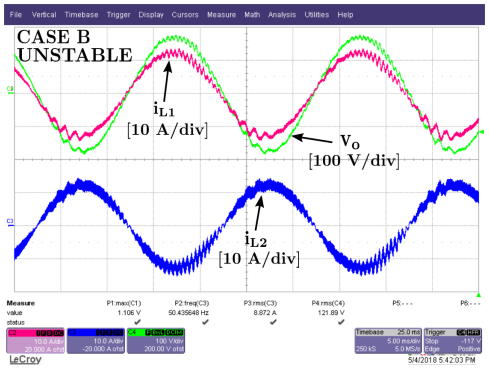

Fig. 13. Experimental data [5 ms/div] - CASE B. Currents: pink - i_{L1}, blue - i_{L2}; voltage: green - v_o - steady-state waveforms with SMU off.

approach is the possibility to include in the analysis any number of harmonic components, just by setting the truncation order. Furthermore, due to the structure of the HTF operator, the interaction between harmonics is automatically taken into account. This can be achieved also by the Graph Flow based Harmonic Linearisation, or by the Dynamic Phasor method were multiple frequencies are considered. However, in these cases the mathematical derivation becomes a significant constraint and is not always a feasible solution.

One drawback of the proposed Harmonic Impedance measurement method, in its present implementation, is the large number of injections required to obtain accurate LTP Nyquist plots. Nevertheless, at this stage of the research this is not considered a critical limitation since the main goal of the work is to prove the feasibility of the method. Also, in any practical implementation, a stability monitoring system is not likely to run continuously but rather to assess stability at specific discrete time intervals, reducing the impact of a measurement delay. If needed, there are several approaches that can be investigated in order to improve the measurement process, making it faster and computationally more effective. Among all the possible solutions, potential candidates are the injection of a transient to determine the impedance [26], the use of wavelets [27] or impedance measurement techniques based on neural networks [28].

VI. Conclusions

This paper has presented a set of experimental results on a 5 kW single-phase two-converter AC network to validate the black-box stability analysis method based on Harmonic Impedance measurements and LTP Nyquist Criterion originally proposed in [21]. The stability assessment is based on the measurement of Harmonic Impedances through the injection of small

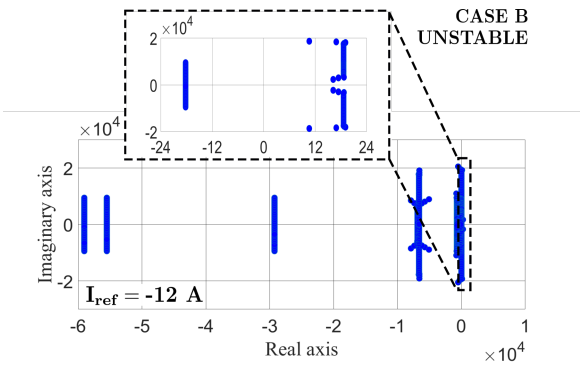

Fig. 14. LTP eigenvalue loci plot from the analytical model - CASE B.

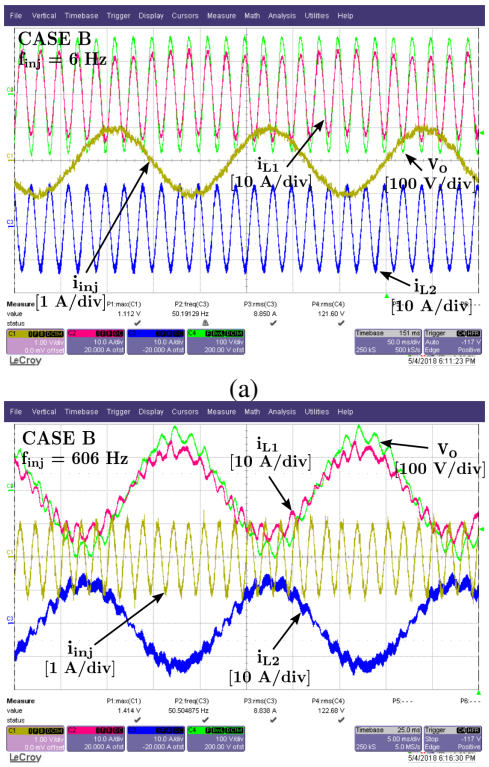

Fig. 15. Experimental data [5 ms/div] - CASE B. Currents: pink - i_{L1}, blue - i_{L2}, yellow - i_{inj}; voltage: green - v_o. Current injection at (a) - 6 Hz; (b) - 606 Hz.

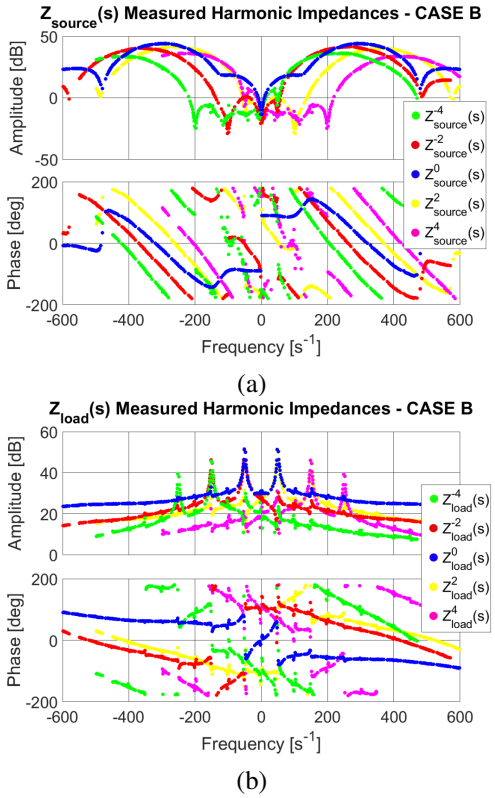

Fig. 16. Experimental data: (a) Source and (b) Load Measured Harmonic Impedances - CASE B.

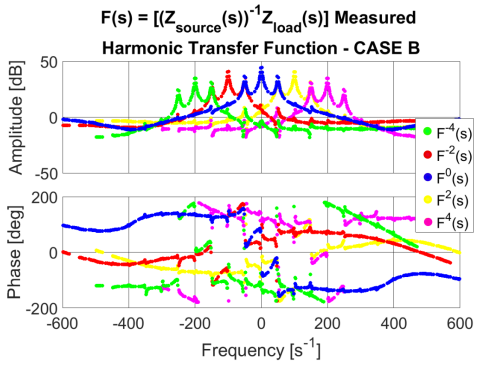

Fig. 17. Experimental data: measured Open-Loop HTF $\mathcal{F}(s)$ - CASE B.

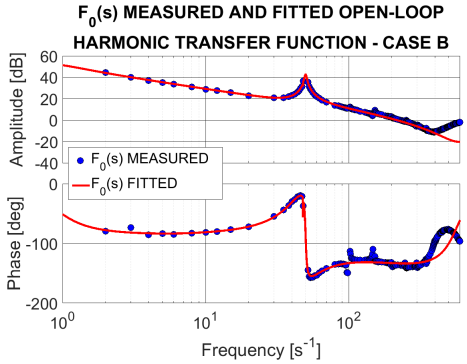

Fig. 18. Experimental data: measured (dots) and fitted (line) Open-Loop HTF $\mathcal{F}_0(s)$ - CASE B.

current perturbations by an external converter, the SMU (Stability Measurement Unit) whose controller defines the required current injections and stores the measured load/source voltage and current perturbations. Stored data are then post-processed in Matlab to assess stability. The method does not require the knowledge of the system parameters, relying only on injections and measurements. However, to evaluate the quality of the black-box stability assessment, an analytical prediction is also performed based on the nominal design parameters. The experimental results, shown for a stable and an unstable operating condition, demonstrated the feasibility of the method and its good match with the analytical prediction, despite the simplicity of the proposed implementation.

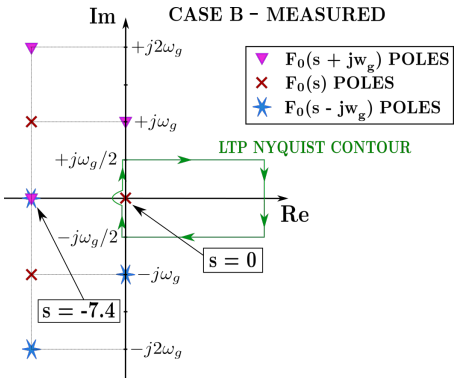

Fig. 19. Experimental data: measured poles location of the Open-Loop HTF $\mathcal{F}_0(s)$ - one pole inside the LTP Nyquist Contour - CASE B.

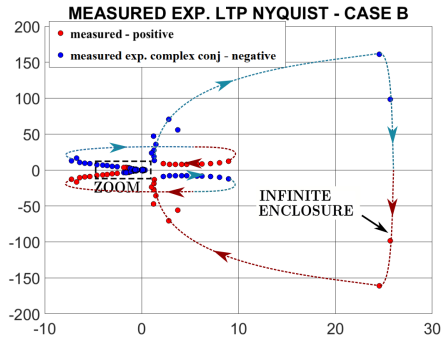

(a)

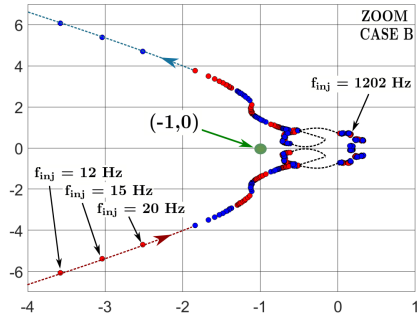

(b)

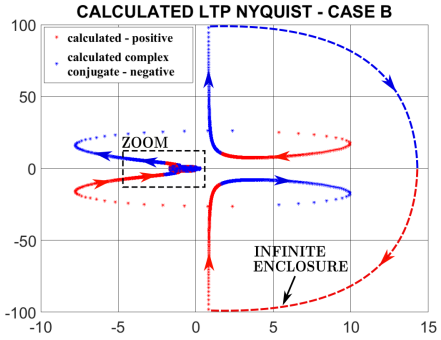

(c)

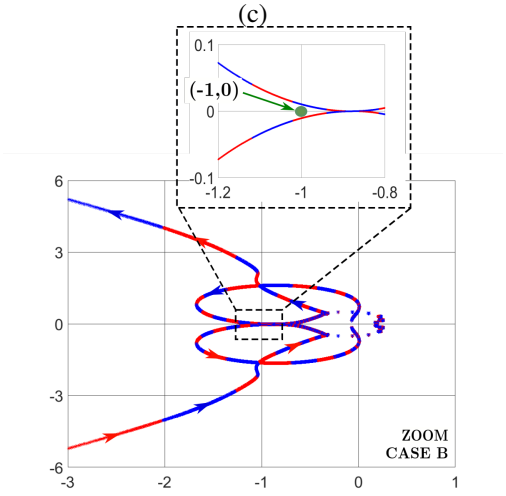

(d)

Fig. 20. (a)-(b) Measured LTP Nyquist plot and (c)-(d) analytical prediction of the LTP Nyquist plot. No counterclockwise encirclements of the critical point - unstable system - CASE B.

REFERENCES

[1] J. H. R. Enslin and P. J. M. Heskes, "Harmonic interaction between a large number of distributed power inverters and the distribution network," *IEEE Trans. Power Electron.*, vol. 19, no. 6, pp. 1586–1593, Nov. 2004.

[2] F. Blaabjerg, R. Teodorescu, M. Liserre, and A. V. Timbus, "Overview of control and grid synchronization for distributed power generation systems," *IEEE Trans. Ind. Electron.*, vol. 53, no. 5, pp. 1398–1409, Oct. 2006.

[3] R. D. Middlebrook, "Input filter considerations in design and application of switching regulators," in *Proc. IEEE Ind. Appl. Soc. Annu. Meeting*, pp. 366–382, 1976.

[4] M. Belkhayat, *Stability Criteria for AC Power Systems with Regulated Loads*. PhD thesis, Purdue University, Dec. 1997.

[5] A. G. J. MacFarlane and I. Postlethwaite, "The generalized Nyquist stability criterion and multivariable root loci," *Int. J. Control*, vol. 25, no. 1, pp. 81–127, 1977.

[6] J. Sun, "Small-signal methods for AC distributed power systems; a review," *IEEE Trans. Power Electron.*, vol. 24, pp. 2545–2554, Nov 2009.

[7] M. Cespedes and J. Sun, "Impedance modeling and analysis of grid-connected voltage-source converters," *IEEE Trans. Power Electron.*, vol. 29, no. 3, pp. 1254–1261, March 2014.

[8] T. Yang, S. Bozhko, J. M. Le-Peuvedic, G. Asher, and C. I. Hill, "Dynamic phasor modeling of multi-generator variable frequency electrical power systems," *IEEE Trans. Power Syst.*, vol. 31, no. 1, pp. 563–571, Jan. 2016.

[9] B. Wen, R. Burgos, D. Boroyevich, P. Mattavelli, and Z. Shen, "AC stability analysis and *dq* frame impedance specifications in power-electronics-based distributed power systems," *IEEE J. Emerg. Sel. Top. Power Electron.*, vol. 5, no. 4, pp. 1455–1465, Dec. 2017.

[10] S. Shah and L. Parsa, "Impedance modeling of three-phase voltage source converters in dq, sequence, and phasor domains," *IEEE Trans. Energy Convers.*, vol. 32, no. 3, pp. 1139–1150, Sept. 2017.

[11] A. Rygg, M. Molinas, C. Zhang, and X. Cai, "On the equivalence and impact on stability of impedance modeling of power electronic converters in different domains," *IEEE J. Emerg. Sel. Top. Power Electron.*, vol. 5, no. 4, pp. 1444–1454, Dec. 2017.

[12] X. Wang, L. Harnefors, and F. Blaabjerg, "Unified impedance model of grid-connected voltage-source converters," *IEEE Trans. Power Electron.*, vol. 33, no. 2, pp. 1775–1787, Feb. 2018.

[13] J. Kwon, X. Wang, F. Blaabjerg, C. L. Bak, V. S. Sularea, and C. Busca, "Harmonic interaction analysis in a grid-connected converter using harmonic state-space (HSS) modeling," *IEEE Trans. Power Electron.*, vol. 32, no. 9, pp. 6823–6835, Sept. 2017.

[14] S. Lissandron, L. D. Santa, P. Mattavelli, and B. Wen, "Experimental validation for impedance-based small-signal stability analysis of single-phase interconnected power systems with grid-feeding inverters," *IEEE J. Emerg. Sel. Top. Power Electron.*, vol. 4, no. 1, pp. 103–115, March 2016.

[15] J. Sun and K. Karimi, "Small-signal input impedance modeling of line-frequency rectifiers," *IEEE Trans. Aerosp. Electron. Syst.*, vol. 44, pp. 1489–1497, Oct 2008.

[16] A. Rygg and M. Molinas, "Apparent impedance analysis: A small-signal method for stability analysis of power electronic-based systems," *IEEE J. Emerg. Sel. Top. Power Electron.*, vol. 5, no. 4, pp. 1474–1486, Dec. 2017.

[17] S. Shah and L. Parsa, "On impedance modeling of single-phase voltage source converters," in *2016 IEEE Energy Conversion Congress and Exposition (ECCE)*, pp. 1–8, 18-22 Sept. 2016.

[18] J. B. Kwon, X. Wang, F. Blaabjerg, C. L. Bak, A. R. Wood, and N. R. Watson, "Harmonic instability analysis of a single-phase grid-connected converter using a harmonic state-space modeling method," *IEEE Trans. Ind. Appl.*, vol. 52, no. 5, pp. 4188–4200, Sept.-Oct. 2016.

[19] V. Salis, A. Costabeber, S. Cox, P. Zanchetta, and A. Formentini, "Stability boundary analysis in single-phase grid-connected inverters with PLL by LTP theory," *IEEE Trans. Power Electron.*, vol. 33, pp. 4023–4036, May 2018.

[20] V. Salis, A. Costabeber, S. M. Cox, A. Formentini, and P. Zanchetta, "Stability assessment of high-bandwidth dc voltage controllers in single-phase active-front-ends: LTI vs LTP models," *IEEE J. Emerg. Sel. Top. Power Electron.*, vol. PP, no. 99, pp. 1–1, 2018.

[21] V. Salis, A. Costabeber, S. M. Cox, and P. Zanchetta, "Stability assessment of power-converter-based AC systems by LTP theory: Eigenvalue analysis and harmonic impedance estimation," *IEEE J. Emerg. Sel. Top. Power Electron.*, vol. 5, pp. 1513–1525, Dec. 2017.

[22] S. R. Hall and N. M. Wereley, "Generalized Nyquist stability criterion for linear time periodic systems," in *American Control Conference, 1990*, pp. 1518–1525, May 1990.

[23] N. M. Wereley and S. R. Hall, "Frequency response of linear time periodic systems," in *Decision and Control, 1990., Proceedings of the 29th IEEE Conference on*, pp. 3650–3655 vol.6, Dec 1990.

[24] B. Gustavsen and A. Semlyen, "Rational approximation of frequency domain responses by vector fitting," *IEEE Transactions on Power Delivery*, vol. 14, no. 3, pp. 1052–1061, Jul 1999.

[25] B. Gustavsen, "Improving the pole relocating properties of vector fitting," *IEEE Transactions on Power Delivery*, vol. 21, no. 3, pp. 1587–1592, July 2006.

[26] M. Sumner, B. Palethorpe, D. W. P. Thomas, P. Zanchetta, and M. C. D. Piazza, "A technique for power supply harmonic impedance estimation using a controlled voltage disturbance," *IEEE Trans. Power Electron.*, vol. 17, no. 2, pp. 207–215, Mar 2002.

[27] M. Sumner, A. Abusorrah, D. Thomas, and P. Zanchetta, "Real time parameter estimation for power quality control and intelligent protection of grid-connected power electronic converters," *IEEE Trans Smart Grid*, vol. 5, no. 4, pp. 1602–1607, July 2014.

[28] P. Xiao, G. K. Venayagamoorthy, K. A. Corzine, and J. Huang, "Recurrent neural networks based impedance measurement technique for power electronic systems," *IEEE Trans. Power Electron.*, vol. 25, no. 2, pp. 382–390, Feb. 2010.

[29] J. Huang, K. A. Corzine, and M. Belkhayat, "Small-signal impedance measurement of power-electronics-based ac power systems using line-to-line current injection," *IEEE Trans. Power Electron.*, vol. 24, no. 2, pp. 445–455, Feb. 2009.

[30] V. Valdivia, A. Lázaro, A. Barrado, P. Zumel, C. Fernández, and M. Sanz, "Impedance identification procedure of three-phase balanced voltage source inverters based on transient response measurements," *IEEE Trans. Power Electron.*, vol. 26, no. 12, pp. 3810–3816, Dec. 2011.

[31] X. Yue, Z. Fang, F. Wang, Z. Zhang, and H. Shi, "A novel adaptive frequency injection method for power electronic system impedance measurement," *IEEE Trans. Power Electron.*, vol. 29, no. 12, pp. 6700–6711, Dec. 2014.